Polymer grafted particles: Architectural effects on the dynamics

ARTICLE · MARCH 2009

READS
34

6 AUTHORS, INCLUDING:

Panayiotis Voudouris
Unilever
13 PUBLICATIONS **112** CITATIONS
SEE PROFILE

Jihoon Choi
Chungnam National University
26 PUBLICATIONS **344** CITATIONS
SEE PROFILE

Michael R Bockstaller
Carnegie Mellon University
94 PUBLICATIONS **2,281** CITATIONS
SEE PROFILE

Effect of Shell Architecture on the Static and Dynamic Properties of Polymer-Coated Particles in Solution

Panayiotis Voudouris,[†] Jihoon Choi,[‡] Hongchen Dong,[§] Michael R. Bockstaller,[‡] Krzysztof Matyjaszewski,[§] and George Fytas*[,†,||]

Departments of Chemistry and Materials Science, University of Crete and Technology and FORTH, 71110 Heraklion, Greece; Department of Materials Science and Engineering, Carnegie Mellon University, 5000 Forbes Ave., Pittsburgh, Pennsylvania 15213; Department of Chemistry, Carnegie Mellon University, 4400 Fifth Ave., Pittsburgh, Pennsylvania 15213; and Max Planck Institute for Polymer Research, Ackermannsweg 10, 55128 Mainz, Germany

Received December 30, 2008; Revised Manuscript Received February 9, 2009

ABSTRACT: A quantitative comparison of the effect of the architecture of polymer grafts on the static and dynamic properties of polymer-functionalized colloidal systems in good solvents is presented. Polystyrene-coated silica particle brush model systems exhibiting identical hard core diameter but distinct polymer-shell architectures corresponding to the concentrated and intermediate brush regime were synthesized using atom transfer radical polymerization (ATRP) and studied using static and dynamic light scattering. Both particle systems conform to a core−shell-like form factor, and single self-diffusion is observed in the limit of dilute concentrations. Despite the significantly larger hydrodynamic radius of the intermediate brush particles, the onset of liquidlike structure formation is observed at about equal particle concentration for both systems, indicating the "soft" star-polymer-type interactions of intermediate brush particles. The comparison with the structure and the hydrodynamic factors of hard-sphere suspensions underlines the significant interpenetration of the grafted polymer chains for the particles in the intermediate brush regime. In particular, for semidilute concentrations the threshold concentration for graft-polymer interpenetration of dense particle brushes (evidenced by the emergence of a fast cooperative relaxation mode and a slow particle self-diffusion) is found to be increased by about an order of magnitude as compared to the intermediate brush analogue. The pronounced effect of the architecture of grafted polymer shells on the concentration dependence of the osmotic pressure and dynamic characteristics of particle suspensions illustrates the rich and hitherto unexplored parameter space that determines the organization of particles in suspension and provides insight into the origin of subtle effects related to polymer functionalization that have been observed previously in the crystallization of colloidal systems.

I. Introduction

Current interest in hybrid core−shell particle systems consisting of a hard (inorganic) core and a soft (polymer) corona is driven by two major motivations: First, from a fundamental perspective, the hard−soft characteristics of particle core and shell render these materials an intermediate state between hard particulate systems as well as soft star polymers. While for hard spheres the static and dynamic properties are mostly determined by entropy-driven transitions, structure formation in star polymers is predominantly determined by excluded volume interactions and chain configurational entropy.[1−4] The study of the static and dynamic properties of polymer-grafted nanoparticles and colloids thus offers the opportunity to elucidate the respective relevance of the various parameters that contribute to the equilibrium structures and phase transitions in particulate systems. The subtle implications of core/shell architecture on the structure formation of core−shell particle systems were highlighted recently by Fukuda and co-workers. They demonstrated for the particular case of the crystallization of poly(methyl methacrylate)-grafted silica colloids a transition from random HCP/FCC to predominantly FCC ordering with increasing molecular weight of the surface-grafted polymer ligands.[5] An earlier work on poly(dimethylsiloxane)-grafted silica provided evidence for the distinct effect of architecture on the dependence of the collective diffusion of particle brushes on the structure and hydrodynamics as compared to hard-sphere systems.[6] From a more application-oriented point of view, polymer-grafted nanoparticles and colloidal systems are at the core of the development of novel material technologies such as photonic or nanocomposite materials that will benefit from a better understanding of the relevant parameters that determine structure formation processes and kinetics in these systems.[7,8]

The synthetic challenges associated with the precise control of grafting density, molecular weight, and narrow polydispersity of polymers grafted to a particle surface have rendered studies of the static and dynamic properties of inorganic/organic core−shell particles difficult. Recent progress in the use of controlled radical polymerization, in particular atom transfer radical polymerization (ATRP), holds the promise to overcome these challenges and to provide well-defined polymer−particle model systems in which the soft/hard characteristics can be tuned over a wide range.[9−11] For example, we previously demonstrated the synthesis of polystyrene-coated silica particles (PS@SiO_2) with precise control of grafting density, molecular weights of the surface grafted ligands up to about 100 kg/mol and polydispersity index of PDI $\sim$ 1.2 using ATRP.[12] The high level of architectural control facilitated by these novel synthetic techniques gives rise to new opportunities for the exploration of the interrelationship between particle architecture and the static as well as dynamic properties of hybrid core/shell particle systems. For the purpose of the present paper two major types of particle architecture will be distinguished dependent on the density and conformation of surface-bound polymer chains: (1) the concentrated brush regime, characterized by high grafting densities σ resulting in stretched conformations of the grafted chains, and (2) the intermediate brush regime, characterized by

* To whom correspondence should be addressed.
[†] University of Crete and Technology and FORTH.
[‡] Department of Materials Science and Engineering, Carnegie Mellon University.
[§] Department of Chemistry, Carnegie Mellon University.
[||] Max Planck Institute for Polymer Research.

10.1021/ma802878r CCC: $40.75
Published on Web 03/12/2009

Scheme 1. Illustration of the Brush Regimes of Particle Systems in This Study: Concentrated Brush Regime Characterized by Thickness of the Grafted Layer $L \sim N$ and the Intermediate Brush Regime Characterized by $L \sim N^{0.5}$ (Assuming Ideal Chain of N Monomers)[a]

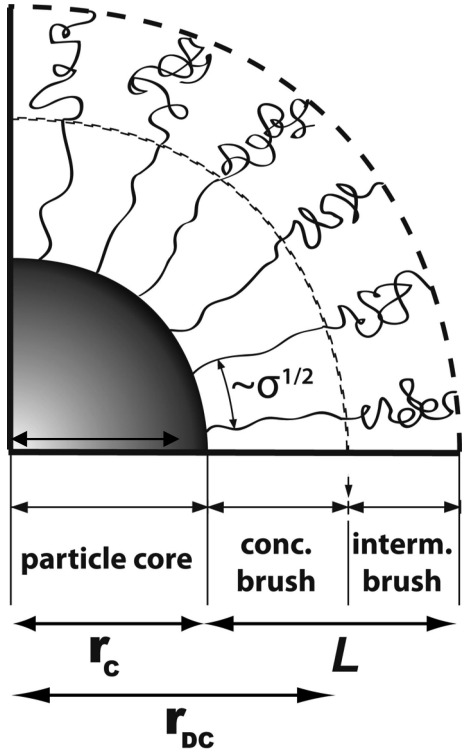

[a] The transition between both regimes occurs at the critical distance r_{DC} (see text for more details). For the present study the particle core radius is $r_c = 10$ nm.

a reduced grafting density and relaxed polymer conformations. Since for spherical particle brushes the effective grafting density decreases with increasing distance r from the particle surface according to $\sigma_{eff} = \sigma_0(r_c/r)^2$, where r_c denotes the particle core radius and σ_0 is the grafting density at the core surface, a transition from the concentrated to the intermediate brush regime is expected at a critical distance r_{DC}. The latter was first proposed by Daoud−Cotton for star polymer systems as $r_{DC} = 2vr_c(\pi\sigma^*)^{1/2}$, with $\sigma^* = \sigma_0 a^2$ denoting the dimensionless surface coverage (a is the monomer length) and v the excluded volume parameter that is about b/a (b is the Kuhn segment) for athermal solvents.[13] In this case, when f chains are grafted on the surface of the particle core, $\sigma_0 = f/(4\pi r_c^2)$ and $r_{DC} \approx bf^{1/2}$. This situation is illustrated in Scheme 1.

Here we present a combined static and dynamic light scattering study of PS@SiO_2 particle solution systems in which grafting density and molecular weight of the surface bound ligand have been tuned such as to afford concentrated and intermediate brush densities. These two regimes are shown to be differentiated by the extent of interpenetration between the chains of two PS@SiO_2 particles. The distinct geometrical constraints related to the curvature of the spherical brushes drives the formation of a depletion region ($\sim r_{DC}$) due to hindered interarm mixing.[14,15] The two PS@SiO_2 systems with the same core radius $r_c = 10$ nm but different number of PS chains ($f = 628$, 1056) exemplify the two regions in Scheme 1 since $r_{DC}/L \sim 0.3$ ($f = 628$) and about 1 ($f = 1056$) where L is the shell thickness (see section IVB). The different packing environments of polymer chains grafted to the particle's surface are furthermore shown to give rise to distinctively different dynamic response above a threshold concentration that provides insight into the effect of polymer grafts on the order formation in particle systems. So far the knowledge on the dynamic structure of core−shell particles was limited to starlike micelles formed by diblock copolymers in a selective solvent with or without subsequent cross-linking of the core and multiarm star polymers.[16,17] The present work is the first report on the missing dynamics of hybrid core−shell particles with distinct behavior being intermediate between hard spheres[18] and ultrasoft multiarm stars.[19]

II. Theoretical Background

The particle volume fraction fluctuations $\phi_q(t)$ due to thermal motions at quiescence is best represented by the intermediate scattering function $S(q,t) = \langle\phi_q(0)\phi_q(t)\rangle/\langle\phi_q^2\rangle$ as a function of the wave vector q and time for the spatiotemporal variation of $\phi_q(t)$. For the well-studied systems of hard-sphere colloids and multiarm stars, $S(q,t)$ exhibits similar and distinct features. In dilute solutions, $S(q,t)$ of monodisperse hard spheres and multiarm stars decay exponentially with a diffusive rate $\Gamma = D_s q^2$ where the self-diffusion coefficient D_s at $q = 0$ and $c \to 0$, $D_0 = kT/6\pi\eta R_h$, yields the hydrodynamic radius R_h in a good solvent with shear viscosity, η. In this low concentration limit, the scattered intensity pattern $P(q)$ is determined by the size and shape of the particle. With increasing concentration, the emergence of interactions is manifested in the static structure factor $S(q)$ which in both systems develop a peak corresponding to the average particle distance at a given concentration and in the nonexponential shape of $S(q,t)$. In this interacting regime, the dynamics of hard-sphere colloids are well documented both theoretically and experimentally.[18] The short time diffusion $D_{sh}(q)$ obtained from the initial slope ($t \to 0$) of $S(q,t)$ is affected by both thermodynamic and kinetic forces since it describes the structural relaxation

$$D_{sh}(q) = D_0 H(q)/S(q) \quad (1)$$

where $H(q)$ accounts for the hydrodynamic interactions. In the thermodynamic limit (i.e., $q \to 0$), the structure factor $S(0) \sim (\partial\Pi/\partial c)^{-1}$ relates to the osmotic pressure Π of the suspension and $\phi_q(t)$ decays via collective diffusion with D_c being an increasing function of concentration. In contrast, for monodisperse hard spheres at q corresponding to the first minimum of $S(q)$ (diminished interparticle interactions) or in the presence of size polydispersity (mainly incoherent scattering) irrespectively of q, the self-diffusion coefficient D_s is deduced from the experimental $S(q,t)$. Expectedly, D_s decreases with concentration.

In the case of multiarm star solutions,[19] the star topology breaks the spatial homogeneity of a semidilute solution of linear homopolymers in terms of ϕ due to the presence of two distinct regions: a core with radius d and $\phi(r) = 1$ and a coat of radius r_1 where the arms are strongly stretched and $\phi(r) \sim (d/r)^{4/3}$ decreases with distance reaching the bulk solution concentration ϕ_{eff} at $r \sim r_1$. Thus, the interarm penetration in the semidilute solution proceeds up to about $r_1 < R_S$, with $R_S \sim N^{3/5}f^{1/5}$ being the star radius. For multiarm star solutions above the overlap concentration, $\phi^*_{eff} \sim f^{2/5}N^{-4/5}$, $S(q,t)$ is dominated by the fast cooperative diffusion D_{coop} which increases with ϕ_{eff}/ϕ^*_{eff} stronger than for semidilute solutions of linear polymers due to the enhanced osmotic pressure in the interpenetrated multiarm stars. This process renders the deduction of the collective (structural) diffusion D_c difficult, and only the self-diffusion D_s that originates in the finite variance of both, the grafting density and the degree of polymerization, is unambiguously resolved. The clear contribution of the cooperative diffusion and the weak participation of the structural relaxation in the $S(q,t)$ of semidilute multiarm star solutions distinguishes this system from

Table 1. Molecular Characteristics

sample	M_n[a]	σ (nm^{-2})[b]	f[c]	m(PS)/m(SiO$_2$)[d]	M_w (g/mol)[e]	R_h (nm)[f]
DP150	15.6K	0.84	1056	2.5	2.3×10^7	29
DP770	80.4K	0.5	628	7.5	1.15×10^8	67

[a] Molar mass of tethered PS. [b] Grafting densities of the grafted PS on the surface of the particles. [c] Number of polymer chains grafted on the surface of the particle. [d] Mass composition m(PS)/m(SiO$_2$). [e] Average molecular weight of the core−shell particles. Columns *a*−*e* were reproduced from ref 12. [f] Hydrodynamic radius of the core−shell particles obtained from PCS.

the much better documented case of the hard-sphere suspensions. For the few known cases, it appears that the increase of core radius enhances the contribution of the structural collective diffusion with distinctly different hydrodynamic factor $H(q)$ (eq 1) compared to the suspensions of hard-sphere particles.

III. Experimental Section

Particle Synthesis. All chemicals were purchased from Sigma-Aldrich Co., unless otherwise specified. Silica nanocrystals (particle radius $r_c = 10$ nm) were obtained from Nissan Chemicals (MIBK-ST) and functionalized with the alkyl halide initiator 1-chlorodimethylsilylpropyl 2-bromoisobutyrate according to the procedure described previously.[11] Toluene (ACS, 99.5%) was purchased from Fisher Scientific and purified by distillation and filtration through a 0.2 μm filter before being added to samples. Inhibitor from the styrene monomer was removed by passage through a column filled with basic alumina. Ethyl 2-bromoisobutyrate (EBiB), *N*,*N*,*N*′,*N*″,*N*″-pentamethyldiethylenetriamine (PMDETA), 4,4′-dinonyl-2,2′-bipyridine (dNbpy), copper(II) bromide, copper(II) chloride, tin(II) 2-ethylhexanoate (Sn(EH)$_2$), anisole, and hydrofluoric acid (36%) were used as received from Aldrich. Copper(I) bromide was purified by washing several times with glacial acetic acid and stored (dry) under a blanket of nitrogen. Tris(2-(dimethylamino)ethyl)amine (Me$_6$TREN) was prepared as described elsewhere.[17] Synthesis of the particle systems DP150 and DP770 was performed using normal ATRP and ARGET ATRP techniques, respectively.[20] The particle synthesis has been described in detail in ref 12. No significant amount of homopolymer impurity could be detected in both particle samples after fractionation. Table 1 summarizes the characteristic features of both particle samples. On the basis of the compositional information presented in Table 1, it can be deduced that the particle samples represent the dense brush regime (DP150) and intermediate brush regime (DP770).

Photon Correlation Spectroscopy (PCS). The experimental normalized light scattering intensity ($I(q,t)$) autocorrelation function $G(q,t) \equiv \langle I(q,t)I(q)\rangle/|I(q)|^2$ was recorded over broad time range (10^{-7}−10^3 s) with an ALV-5000 goniometer/correlator setup using an Nd:YAG laser at $\lambda = 532$ nm. The scattering wave vectors $q = (4\pi n/\lambda)\sin(\theta/2)$ with n being the refractive index of the medium and θ the scattering angle was varied in the range between 0.005 and 0.035 nm^{-1}. Under homodyne beating conditions, the desired concentration relaxation function is computed from the experimental $G(q,t)$: $C(q,t) = [G(q,t) - 1]/f^*]^{1/2}$ where $f^* \leq 1$ is an instrumental coherence factor. In the dilute regime, $C(q,t)$ is a single decay function, and the effective short time diffusion coefficient is determined from the initial decay rate of according to[18]

$$D_{Sh}(q) = \frac{\Gamma}{q^2} = \left(\frac{1}{q^2}\right)\lim_{t=0}\left(\frac{d[\ln g^{(1)}(t)]}{dt}\right) \quad (2)$$

where $g^{(1)}(q,t)$ is the normalized relaxation function $C(q,t)$. In this regime, the particle hydrodynamic radius R_h is computed from the translational diffusion $D_0 = D_s(q{=}0, c{\rightarrow}0)$. In the nondilute interacting regime, the presence of multiple relaxation processes the analysis of $C(q,t)$ proceed its inverse Laplace transformation (ILT):

$$C(q,t) = \int L(\ln\tau)\exp(-t/\tau)\, d\ln\tau \quad (3)$$

The distribution of relaxation times $L(\ln\tau)$ can be decomposed as a sum of contributions $L(\ln\tau) = \sum_i L_i(\ln\tau)$, and the scattering intensity associated with the ith process is $I_i(q) = I(q)\int_{\ln\tau} L_i(\ln\tau)\, d\ln\tau$ with $I(q)$ being the total scattering intensity, whereas the relaxation rate Γ_i is obtained from the peak position of $L_i(\ln\tau)$. The ILT analysis yields both the rate Γ_i and the associated intensity I_i, which provide a measure of the efficiency of the particular motional mechanism to relax the density (concentration) fluctuations of the system.[21]

IV. Results

A. Overview. The increase of concentration strongly affects the static and dynamic properties of the present core/shell solutions in a good solvent, and different regimes can be identified by the changes in the form of the structure factor, $S(q) = I(q)/P(q)$, with $P(q)$ being the form factor of the core/shell particle. Three different regimes are recognized in the static and the dynamic properties of the two systems. In the dilute regime I, $S(q) = 1$, the relaxation function $C(q,t)$ exhibits a single-exponential decay describing the particle translational motion, and the scattering intensity $I(q) \sim P(q)$ is a measure of the size and shape of the particle. With increasing particle concentration, $S(q)$ develops a q-dependence that is associated with increasingly complex relaxation characteristics that result in deviations from the single-exponential shape. In the interacting concentrated regime III, more than one relaxation process can clearly be discerned from the shape of the correlation function $C(q,t)$. In order to account for packing effects and to assess the relative contribution of the two main structural characteristics on the static and dynamic properties, i.e., hard-sphere colloidal and ultrasoft multiarm polymer-type behavior, we evaluate the effective volume fraction, $\phi = cN_AV_p/M_w$, from the mass concentration c (g/mL) using the experimental value of the hydrodynamic radius, R_h, for the estimation of the particle volume V_p ($= 4\pi R_h^3/3$); N_A is the Avogadro number.

Figure 1 shows experimental $S(q)$ versus the reduced size qR_h for the DP770/CCl$_4$ system at three concentrations in the different regimes. For concentrations $c < 5.5 \times 10^{-4}$ g/mL, $S(q) = 1$ and the particle solutions are in the dilute noninteracting regime, whereas already at $c \geq 0.01$ g/mL, a liquidlike $S(q)$ (II) is clearly observed. In regime II, the presence of hydrodynamic interactions is manifested in the q dependence of the short time diffusion D_{sh} (section IVC). A rough estimate of the overlap concentration of the DP770 can be obtained from values of $c^* \sim 0.14f^{2/5}N^{-4/5}$ that have been reported previously for polybutadiene multiarm stars with $f = 128$ and degree of polymerization of individual arm segments of $N \sim 130$−1500.[19] Using $f = 628$ and $N = 770$ and neglecting the small fraction of the SiO$_2$ core (fifth column in Table 1), $c^* \sim 0.01$ g/mL, which falls in the vicinity of the crossover regime II; under the same assumption for DP150, $c^* \sim 0.05$ g/mL. With increasing concentration the proximity of the particles shifts the peak position of $S(q)$ outside the window of the light scattering q's, while the osmotic pressure ($\sim 1/S(q{=}0)$ strongly increases. These changes qualitatively modify the dynamics of the system (see below), and hence a new crossover regime III becomes apparent. Based on Figure 1, the characterization of the individual PS@SiO$_2$ is performed in regime I, whereas hydrodynamic and thermodynamic effects become effective in the next two concentration regimes. The operation of three concentration regimes (Figure 1) was found to apply also for DP150 as discussed below.

B. Dilute Regime. The experimental relaxation functions $C(q,t)$ have a single-exponential shape as shown in Figure 2 (solid lines) for the two systems in the dilute regime I at $q = 0.033$ nm^{-1}. The particle self-diffusion $D_0 = \Gamma(q)/q^2$ obtained from the relaxation rate $\Gamma(q)$ of the experimental $C(q,t)$ is found

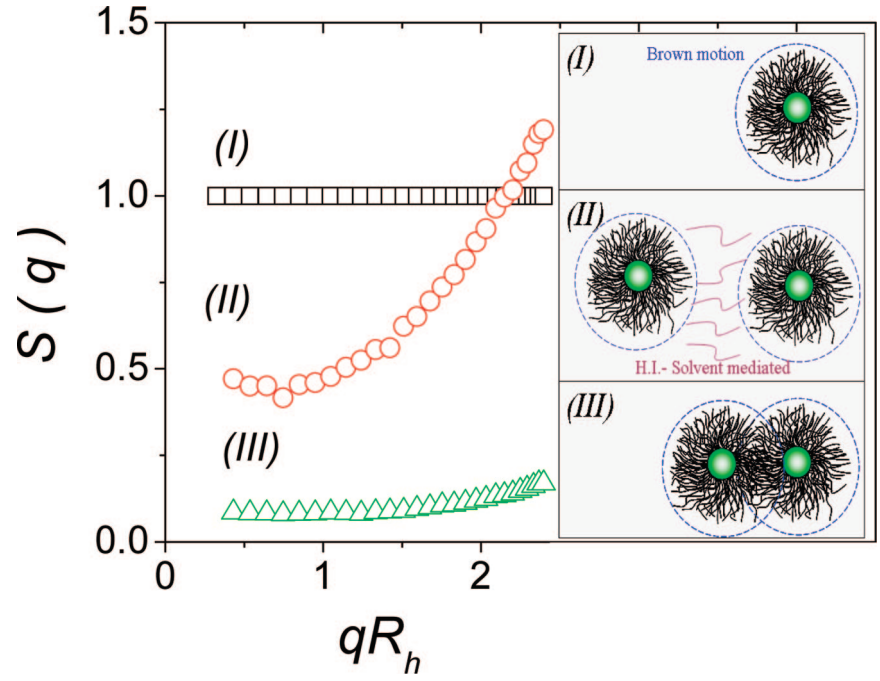

Figure 1. Structure factor $S(q)$ vs qR_h at three different concentration regimes of DP770 in CCl_4. Regime I: dilute noninteracting regime $c \ll c^*$ ($c = 3 \times 10^{-5}$ g/mL). Regime II: dilute interacting regime $c < c^*$ ($c = 7 \times 10^{-3}$ g/mL). Regime III: nondilute interacting regime $c > c^*$ ($c = 0.12$ g/mL). The real space structures in the three regimes are shown schematically in the right panel where H.I. denotes the presence of hydrodynamic interactions on the short time diffusion D_{sh}.

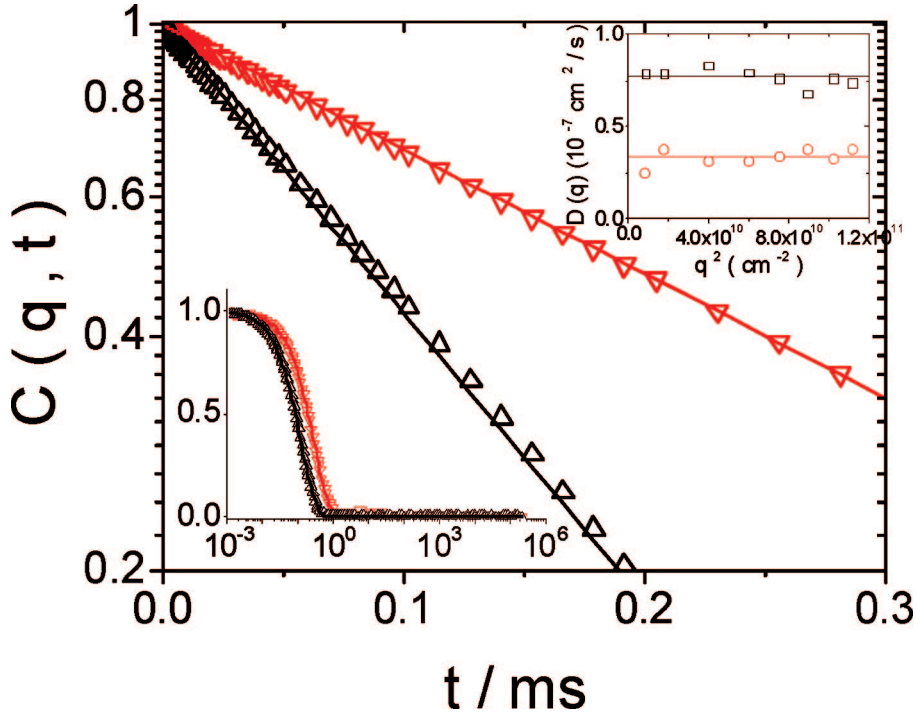

Figure 2. Relaxation functions for the dilute solutions of DP150 (Δ, $c = 1.1 \times 10^{-4}$ g/mL) and DP770 (▽, $c = 3.4 \times 10^{-5}$ g/mL) in CCl_4 at a scattering vector $q = 0.033$ nm^{-1} in two different semilog presentations (main plot and lower inset). Upper inset shows the translational diffusion $D_s(q)$ for DP150 (□) and DP770 (○).

to be q-independent as seen in the upper inset to Figure 2; $D_0 = 7.7 \times 10^{-8}$ cm^2/s for DP150, $D_0 = 3.4 \times 10^{-8}$ cm^2/s for DP770, and the computed values of the hydrodynamic radius R_h are listed in Table 1. In this dilute regime, the static scattering intensity measures the form factor $P(q)$ of the isolated particles. In order to obtain a reliable information on the shell size, we have measured $P(q)$ of the two PS@SiO_2 particles in two good solvents (toluene, CCl_4) which weigh differently the core and shell contribution to the total scattering intensity because of their different optical contrast. Figure 3 shows the experimental absolute Rayleigh ratio $R(q)/c$ for the two particles in the two solvents. The normalized form factor $P(q) = R(q)/R(q=0)$, also shown in Figure 3, is based on the value of $R(q=0)$ obtained from the intercept of $1/R(q)$ vs q^2, which is linear at low q's. The ratio of the $R(q=0)$ for the DP770 and DP150 expectedly compares well with the ratio (≈5) of their molecular weights listed in Table 1. The form factor $P(q)$ is represented by the core−shell model equation:[13,22−24]

$$P(q) = [b_c F_c(q, r_c) + b_s F_s(q, r_c, R_p)]^2 \quad (4)$$

where b_c and b_s are the contrast factors for the core (c) and shell (s) with core radius r_c and overall core−shell radius R_p, and $F_c(q)$ and $F_s(q)$ are the scattering amplitudes of the core and shell, respectively. Note that $F_s(q)$ is computed for the assumption of a hyperbolic density distribution of a starlike structure i.e., $\phi(r) \sim r^{-4/3}$. Since the refractive index profile that controls the contributions b_c and b_s is different in the two solvents, the scattering from the DP150 is stronger in toluene than in CCl_4 due to the larger contribution of the silica core in the former solvent. Using $r_c = 10$ nm for the SiO_2 core radius with no polydispersity, the PS thickness L in both good solvents assumes $L = 26 \pm 2$ and 60 ± 3 nm in DP150 and DP770, respectively; the size of the core was confirmed by small-angle X-ray scattering from dilute solutions of DP150. The shape of $P(q)$, however, depends on the choice of the solvent due to its different optical contrast with the core and shell. Noteworthy is the difference between the R_g values in the two solvents obtained from the Ornstein−Zernike relation, $1/R(q) = (1 + q^2R_g^2/3)/R(q=0))$, that weighs more the constituent with the stronger scattering. Thus, the fact that the value of L deduced from the fit of eq 4 to the experimental $P(q)$ is the same in both good solvents supports the analysis and assures a reliable assessment of the structure factor $S(q) = I(q)/P(q)$ in the interacting regime examined below.

In the Daoud−Cotton multiarm star model[13] with f arms and N degree of polymerization per arm the end-to-end distance in good solvents is given by

$$R = bN^{\nu}f^{(1-\nu)/2} \quad (5)$$

This expression captures the experimental value of the thickness, $L = R/6^{1/2}$, using for the Kuhn segment $b = 0.81 \pm 0.02$ nm for both PS@SiO_2 particles.

C. Dilute Interacting Regime. The intermediate scattering functions $C(q,t)$ progressively deviate from the simple exponential shape of Figure 2, but still only one process is present. This indicates the formation of a liquidlike structure (regime II in Figure 1), and the solutions reflect particle-like behavior reminiscent of noncrystalline colloidal suspensions; there is no significant overlap between PS ligands on neighboring PS@SiO_2. As for the hard-sphere colloids, the analysis proceeds through the first cumulant representation (eq 2). The normalized short time diffusion coefficient, $D_{sh}(q)/D_0$, where $D_{sh}(q) = \Gamma(q)/q^2$, is found to decrease with the probing wave vector q, as shown in Figure 4a. This slowing down is observed for the PS@SiO_2 solutions in both solvents. Concurrently, these solutions exhibit a liquidlike $S(q)$ with a peak at finite q falling barely within the experimental q window (Figure 4b). According to eq 1, the slowing down of $D_{sh}(q)$ at finite q's is partially due to the increase of $S(q)$ and the nonlocal nature of the hydrodynamic interactions (Figure 4c). We note that the observed changes in the dynamics and thermodynamics of both systems in concentration regime II are reminiscent of particulate suspensions and illustrate the distinction of suspensions of polymer-coated particles to solutions of homopolymers. Figure 4 depicts the experimental $S(q)$ and $H(q)$ with predictions for hard-sphere colloidal suspensions at ϕ_{HS}.[18,25] At the same volume fraction ($\phi_{HS} = \phi$), it clearly fails (dashed lines) to approximate the $S(q)$ of the present suspensions. However, the situation is significantly changed when a comparison is attempted at higher volume fraction of the hard-sphere suspensions (solid lines in Figure 4b,c). For the DP150 system, an increase of ϕ by 25% suffices for the observed similarity with hard-sphere suspensions. On the contrary, the DP770 system at ϕ would be reminiscent of a much denser hard spheres suspension at $\phi_{HS} \sim 2.5\phi$. Such discrepancy between ϕ_{HS} and ϕ in the case of DP770 underlines its soft starlike nature, allowing for the onset of interactions at relatively low volume fractions.[14,26,27] In fact, above about $\phi = 0.07$, the relaxation function $C(q,t)$ becomes complex (see Figure 6). On the other hand, the disparity between ϕ_{HS} and ϕ is significantly reduced, in the case of the densely grafted DP150 particle.

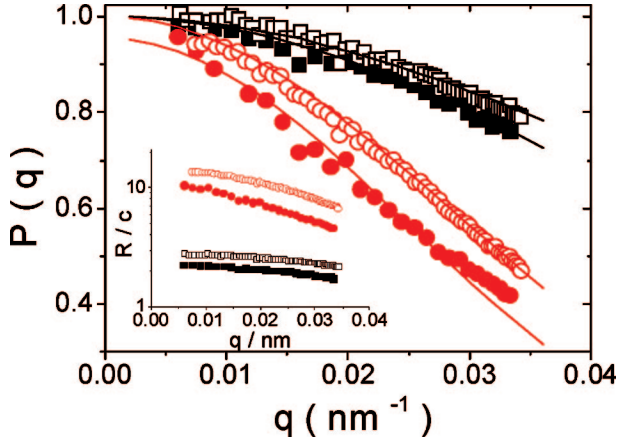

Figure 3. Form factor $P(q)$ and reduced Rayleigh ratio R/c (inset) in carbon tetrachloride (solid symbols) and in toluene (open symbols) for DP150 (□) at volume fraction $c = 1.1 \times 10^{-4}$ g/mL and for DP770 (○) at volume fraction $c = 3.4 \times 10^{-5}$ g/mL. Solid lines denote the fits of eq 4 to the experimental data.

Up to about 0.01 g/mL, the static and dynamic properties of the two PS@SiO_2 particle solutions are qualitatively similar. Above about this concentration, the solution thermodynamics significantly alter with increasing concentration as seen in the variation of the total scattering intensity $R(q=0)$ in the main plot of Figure 5. A strong decrease of the intensity occurs at about $\phi^* \sim 0.04$ for both PS@SiO_2 particles. The magnification of the shaded area in Figure 5 presented in the inset depicts the two different slopes at the crossover concentration. The first weak decrease of $R_{q=0}(c)$ with concentration is compatible with favorable polymer layer−solvent interactions with positive second virial coefficient.

A second strong reduction of $R_{q=0}(c)$ that is observed above ϕ^* signals the significant enhancement of the osmotic pressure which is expectedly stronger in DP770 suspensions. In the next section the implications of the enhanced interactions on the dynamic properties in this third concentration regime will be discussed.

D. Nondilute Interacting Regime. The concentration regime above ϕ^* is characterized by the appearance of multiple relaxation processes in $C(q,t)$. Figure 6 shows the experimental $C(q,t)$ at two probing wave vectors for the two systems in CCl_4 in the nondilute interacting regime III. The broad shape of $C(q,t)$ extending over more than 3 decades is uniquely represented by eq 3. The analysis yields three distinct relaxation processes (upper inset in Figure 6) characterized by physical meaningful relaxation rates and amplitudes as documented by their wave vector dependence (lower insets in Figure 6) for both systems. The rates for all three processes are diffusive, and the associated intensities represent the total intensity $R(q)$ in Figure 5. Note the much weaker intensity of the fastest process (1) and the increase of the intensities for the other two processes at high q's which suggests their association with $S(q)$.

The diffusion coefficients normalized to the limiting D_0 value are plotted as a function of particle volume fraction over a broad range in Figure 7. In regime I, the long wavelength value of $D_s(q=0)$ (cf. Figure 4) decreases with concentration up to about ϕ as seen in the magnified plot in the inset to Figure 7 for both

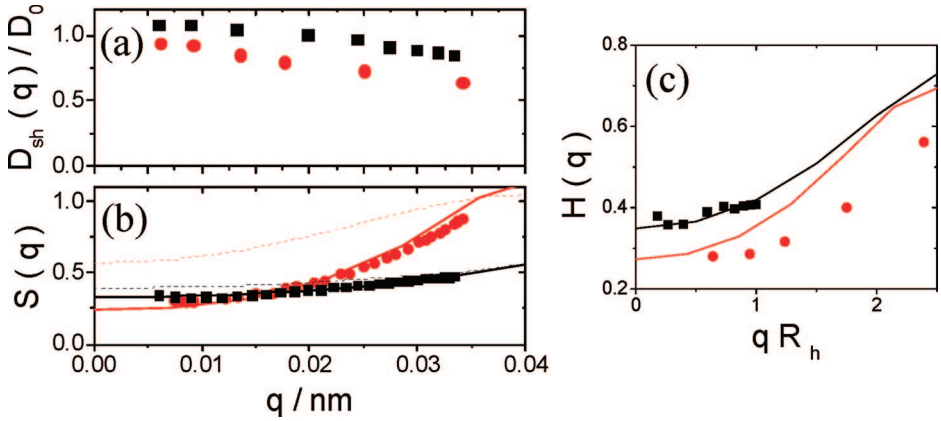

Figure 4. Collective diffusion $D_{sh}(q)$ normalized to D_0 (a) and the structure factor $S(q)$ (b) for DP150 (■) and DP770 (●) in toluene at $c = 0.017$ g/mL ($\phi = 0.11$) and 0.024 g/mL ($\phi = 0.072$).The dashed lines are the Percus−Yevick (PY) predictions for hard spheres at the same volume fractions for DP150 (black dashed line) and for DP770 (red dashed line) while the corresponding solid lines denote the PY predictions for DP150 at $\phi = 0.14$ and DP770 at $\phi = 0.18$. (c). The hydrodynamic factor $H(q) = D(q)S(q)$ (symbols) for DP150 (□) and DP770 (●) at the same concentrations along with the (solid lines) theoretical predictions from Beenaker and Mazur[25] at $\phi = 0.14$ and $\phi = 0.18$, respectively.

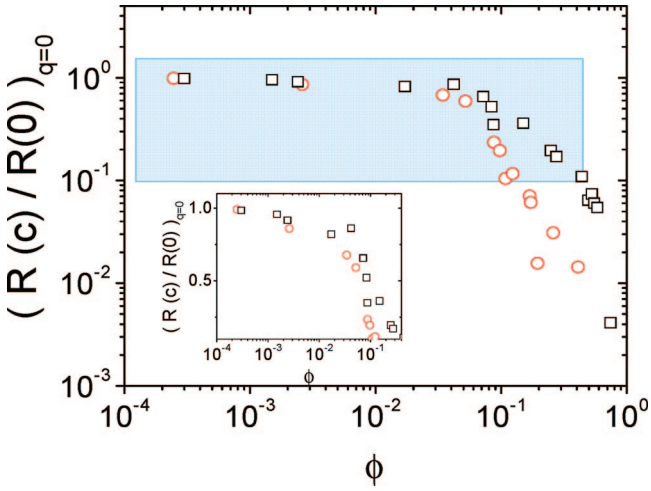

Figure 5. Normalized Rayleigh intensity ratios $R(q=0)$ as a function of the volume fraction ϕ for DP150 (□) and DP770 (○) in CCl_4 at 20 °C. The inset shows in magnification the shaded area in the main plot keeping the same color and symbols for the two systems.

samples. In this regime at $q = 0$, the short-range self-diffusion coefficient equals D_s, since $D(q)$ is independent of q and the solutions do not exhibit liquidlike structure, i.e., $S(q) \sim 1$. For the present good solvency conditions (inset to Figure 5), this decrease of D_s reflects the increase of the friction coefficient with concentration. For the case of hard-sphere colloidal suspensions, both experimental[28−31] and theoretical[25,32] studies have revealed that the dependence of D_s on the particle volume fraction follows the Batchelor's predictions $D_s/D_0 = 1 - 1.73\varphi + O(\varphi^2)$.[33] As expected, this expression can capture only qualitatively the present experimental behavior seen by the red solid line in the inset of Figure 7, since the comparison is made at the same ϕ value for both hard spheres and the present systems.

For volume fractions above about $\phi = 0.08$, which is notably close to ϕ^* obtained from the static intensities, $D(q=0)$ reverses its concentration dependence following up the abrupt increase of the osmotic pressure (Figure 5). In this crossover regime, as already mentioned, $S(q)$ develops a q dependence, and the $D(q)$ is no longer independent of q. The long wavelength diffusion coefficient $D(q=0)$ cannot be related anymore to the short-range self-diffusion coefficient D_s. Instead, $D(q=0)$ is the collective diffusion D_c. In the case of hard-sphere colloidal suspensions at high volume fractions, several theoretical predictions[25,33] and

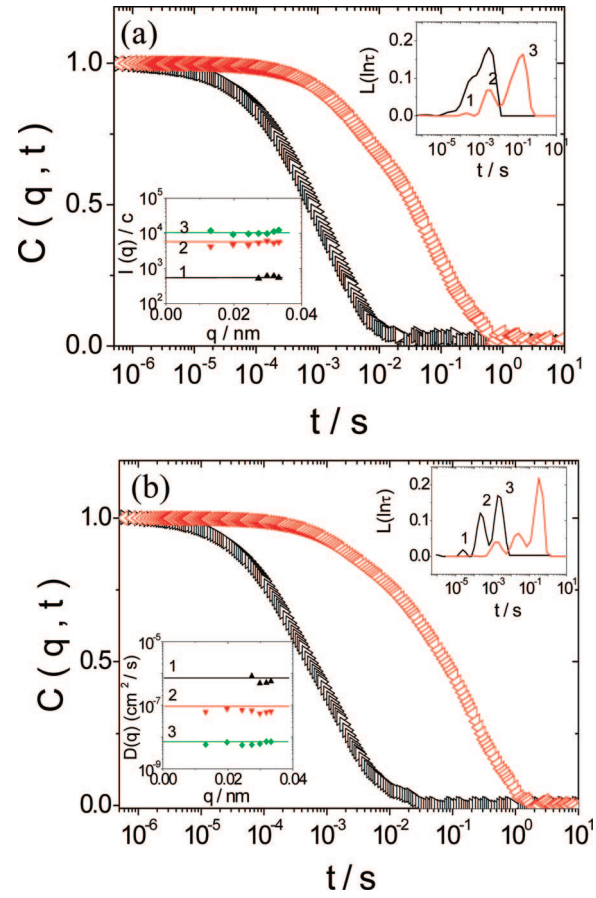

Figure 6. Typical intermediate scattering functions at two scattering wave vector ($q = 0.033$ nm^{-1} (black △) and $q = 0.0089$ nm^{-1} (red △)) for (a) DP150 in CCl4 at volume fraction $\phi = 0.53$ and (b) DP770 in CCl_4 at volume fraction $\phi = 0.15$. Three relaxation processes (1−3) are consistently resolved (inset IL) with q-independent intensities and diffusive rates shown in the insets to (a) and (b), respectively. Lines are to guide the eye.

experimental results[31,34,35] seem to confirm the Bachelor's expression, i.e., $D_c/D_0 = 1 + 1.454\phi - 0.45\phi^2 + O(\phi^3)$,[33] for the collective diffusion directly evolving from the D_0. Again, this expression only qualitatively describes the present D_c data (green dashed line in the inset of Figure 7). The crossover behavior around ϕ^* consistently impacts both static and dynamic

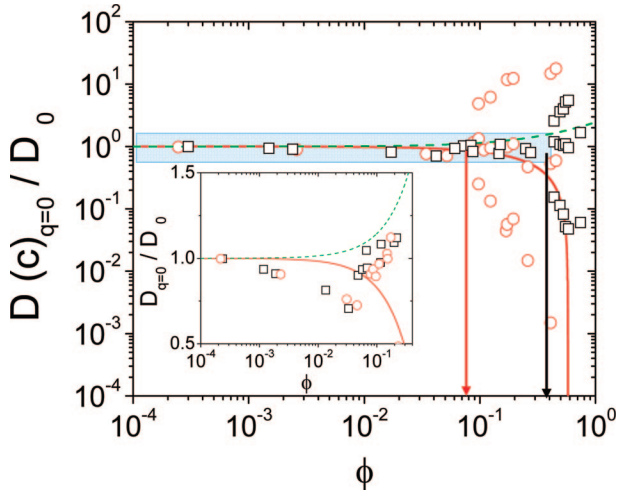

Figure 7. Normalized diffusion coefficients $D(q=0)$ as a function of the volume fraction ϕ for DP150 (□) and DP770 (○) in CCl_4 at 20 °C. The inset shows in magnification the shaded area in the main plot using the same colors and symbols for the two systems. Solid and dashed lines correspond to Batchelor's[33] predictions for the self-and the collective diffusion, respectively. The two arrows indicate the crossover volume fractions (ϕ^{**}) in the two systems.

properties of the two systems. This is, however, not the only feature of the rich dynamics displayed in Figure 7.

For DP770 (intermediate brush regime), two additional diffusive processes appear for ϕ above about 0.08, which is close to ϕ^*. Note that for the denser grafted DP150 this dynamic splitting occurs at $\phi > 0.35$, well above ϕ^*. The dynamics of fastest diffusive process of weak scattering intensity (see Figure 6) increases with increasing concentration, suggesting its origin to be a polymer-like cooperative diffusion (D_{coop}). Strong evidence of the polymeric nature of this fast cooperative diffusion is its absence when an isorefractive to PS solvent ($CHBr_3$) is used. Alternatively, the slowest diffusion that exhibits strong slowing down with concentration is associated with the particle self-diffusion (D_s) which is detected by light scattering due to the finite polydispersity of the PS chains tethered to the SiO_2 cores. This mode is observed in both hard sphere colloids and multiarm star polymers.

V. Discussion

Three pertinent and unexpected findings associated with the dilute and nondilute interaction regime are displayed in Figures 5 and 7: (i) The short time and long wavelength particle diffusion coefficient $D(q=0)$ shows two distinct concentration dependences with an initial decrease up to about ϕ^* and a clear increase above ϕ^*. Based also on the concurrent change in the scattering intensity (inset to Figure 5), this crossover occurs at $\phi^* \approx 0.08$ in both DP770 and DP150 solutions. This implies that the onset of particle dynamic interactions in the two systems with different PS grafts is well captured by the effective volume fraction based on R_h, as seen in the inset of Figure 7. The agreement is less satisfactory for the static properties reflected in the scattering intensities shown in the inset of Figure 5. The different scaling characteristics of the static and dynamic properties of both particle systems are attributed to the different interaction conditions that are prevalent in the respective systems.[14] In particular, the reduced grafting density in case of the DP770 system is expected to allow for stronger chain interpenetration that impact the slowing down of the particle self-diffusion D_s and the appearance of polymer specific cooperative diffusion D_{coop}. In fact, the dynamic splitting into three diffusion processes (see Figures 6 and 7) occurs at volume fraction above but very close to ϕ^* only in the case of DP770.

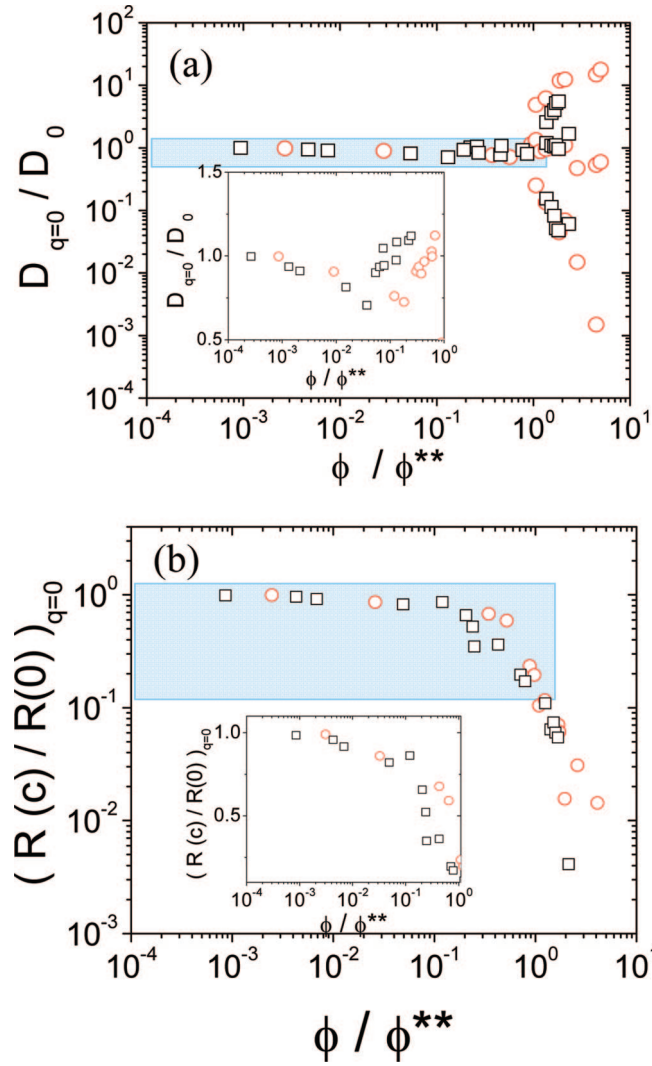

Figure 8. Superposition plots for the normalized diffusion coefficients (a) and scattering intensity (b) based on $\phi^{**} \approx 0.35$ and $\phi^* \approx 0.08$ for DP150 and DP770, respectively. The insets represent magnified view.

On the contrary, DP150 reveals similar splitting with the appearance of D_{coop} at much higher volume fraction $\phi^{**} \sim 0.35$. The polymeric nature of the cooperative diffusion bears analogy to the semidilute solutions of homopolymers which conform to scaling relationships with respect to the overlap concentration. This analogy is illustrated in Figure 8 where $\phi^{**} \sim \phi^*$ was used for DP770. Indeed, the overall satisfactory superimposition indicates that the PS ligand interpenetration in DP150 and DP770 is similar at $\phi \sim \phi^{**}$, which is by a factor of 4.4 higher in the former system.

(ii) The presence of the fastest D_{coop} that speeds up with increasing concentration appears at about the bifurcation concentrations of the particles $D(q=0)$. This polymer-specific process, which was observed previously in solutions of multiarm star polymers, emerges when significant PS grafts interpenetration occurs concurrently with the slowing down of D_s due to the increased viscosity of the system. The appearance at lower ϕ in DP770 than in DP150 corroborates again the notion of much higher degree of PS ligands interpenetration in the former. Hence, the observed superposition of the fast diffusion and the intensity by horizontal shifting of ϕ for DP770 in Figure 8 is not unexpected. We hypothesize that the observed shift in the scaling of the particle self-diffusion by the identical ϕ is due to the solution viscosity which is controlled by the interpenetration as well.

We interpret the shift factor $\alpha \sim 4.4$ that is needed in order to superimpose DP760 self-diffusion and collective diffusion coefficients with those in DP150 as seen in Figure 8 as a consequence of the differences in the brush architecture of the polymer shell of the particles. At $\phi \sim \phi^*$, the outer blob of size $\xi \sim Rf^{-1/2}$ is about twice larger in DP770 (intermediate brush regime, Scheme 1)), and hence arm interpenetration is expected to be more pronounced in DP770 than in DP150 (concentrated brush regime) due to its weaker osmotic pressure ($\sim kT/\xi^3$). For the latter case, a stronger osmotic force is required to enable the interarm overlapping that is fundamental to the activation of the fast cooperative diffusion D_{coop} and to sufficiently increase the solution viscosity for the observed decrease of the particle self-diffusion coefficient. Similarly, the volume fractions (and hence the osmotic pressure $\pi \sim \xi^{-3} \sim \phi$) at which the splitting in the dynamics in both systems is observed differs by about an order of magnitude (see Figure 7). This rationalization is supported by recent theoretical predictions of the forces experienced by two core/shell particles with increased proximity as a function of shell architecture.[14]

VI. Concluding Remarks

The present study provides the first quantitative comparison of the effect of the architecture of polymer grafts on the static and dynamic properties of polymer-functionalized colloidal systems for the particular case of PS@SiO_2 in good solvents. For particles in the intermediate brush regime, significant interpenetration of the grafted polymer chains is observed at concentrations near the overlap concentration, resulting in distinct changes of the dynamic properties, i.e., the slowdown of particle self-diffusion as well as the occurrence of fast cooperative modes related to the relaxation of the interacting polymer brushes (Figure 7). The intermediate brush regime is also manifested at relatively lower particle volume fractions in the structure and the hydrodynamic factors compared to hard-sphere suspensions (Figure 4). For particles in the dense brush regime the increased osmotic interactions are found to increase the threshold concentration for graft interpenetration by about an order of magnitude.

The pronounced effect of the architecture of grafted polymer shells on the concentration dependence of the static and dynamic characteristics of particle suspensions illustrates an up to now unexplored parameter space that determines the organization of particles in suspension and provides insight into the origin for the effect of polymer functionalization on the microstructure formation in colloidal crystal systems. The dynamics of these hybrid core/shell systems exhibit both polymer and hard-sphere colloid specific behavior, which is, therefore, richer and moreover tunable over a broad range of volume fractions. Furthermore, the distinct interactions between dense and intermediate particle brushes that are responsible for the dynamic and static properties of particle suspensions have implications for the mechanical properties of the particles in the solid state—this will be the focus of a forthcoming publication.

Acknowledgment. We thank Professor J. K. G. Dhont for helpful discussions. P.V. thanks GSST (PENED-2003/856) and EU-NANODIRECT CP FP213948-2 for financial support. M.R.B. acknowledges support by NSF (DMR 0706265).

References and Notes

(1) Pusey, P. N.; Vanmegen, W. *Nature (London)* **1986**, *320*, 340.
(2) Kegel, W. K.; van Blaaderen, A. *Science* **2000**, *287*, 290.
(3) Gasser, U.; Weeks, E. R.; Schofield, A.; Pusey, P. N.; Weitz, D. A. *Science* **2001**, *292*, 258.
(4) Yethiraj, A.; van Blaaderen, A. *Nature (London)* **2003**, *421*, 513.
(5) Morinaga, T.; Ohno, K.; Tsujii, Y.; Fukuda, T. *Macromolecules* **2008**, *41*, 3620.
(6) Petekidis, G.; Gapinski, J.; Seymour, P.; van Duijneveldt, J. S.; Vlassopoulos, D.; Fytas, G. *Phys. Rev. E* **2004**, *69*, 042401.
(7) Colvin, V. L. *MRS Bull.* **2001**, *26*, 637.
(8) Bockstaller, M. R.; Mickiewicz, R. A.; Thomas, E. L. *Adv. Mater.* **2005**, *17*, 1331.
(9) Matyjaszewski, K.; Xia, J. H. *Chem. Rev.* **2001**, *101*, 2921.
(10) Braunecker, W. A.; Matyjaszewski, K. *Prog. Polym. Sci.* **2007**, *32*, 93.
(11) Pyun, J.; Jia, S.; Kowalewski, T.; Patterson, G. D.; Matyjaszewski, K. *Macromolecules* **2003**, *36*, 6952.
(12) Bombalski, L.; Dong, H. C.; Listak, J.; Matyjaszewski, K.; Bockstaller, M. R. *Adv. Mater.* **2007**, *19*, 4486.
(13) Daoud, M.; Cotton, J. P. *J. Phys. (Paris)* **1982**, *43*, 531.
(14) Kim, J. U.; Matsen, M. W. *Macromolecules* **2008**, *41*, 4435.
(15) Pakula, T.; Vlassopoulos, D.; Fytas, G. Roovers. *Macromolecules* **1998**, *31*, 8931.
(16) Pyun, J.; Matyjaszewski, K.; Kowalewski, T.; Savin, D.; Patterson, G. D.; Kickelbick, G.; Huesing, N. *J. Am. Chem. Soc.* **2001**, *123*, 9445.
(17) Xia, J. H.; Gaynor, S. G.; Matyjaszewski, K. *Macromolecules* **1998**, *31*, 5958.
(18) Pusey, P. N. In *Colloidal Suspensions in Liquids, Freezing and the Glass Transition, Les Houches Lectures*; Hansen, J. P., Levesque, D., Zinn-Justin, J., Eds.; Elsevier: Amsterdam, 1991.
(19) Semenov, A. N.; Vlassopoulos, D.; Fytas, G.; Vlachos, G.; Fleischer, G.; Roovers, J. *Langmuir* **1999**, *15*, 358.
(20) Jakubowski, W.; Min, K.; Matyjaszewski, K. *Macromolecules* **2006**, *39*, 39.
(21) Fytas, G. In *Scattering. Scattering and Inverse Scattering in Pure and Applied Science*; Pike, R., Sabatier, P., Eds.; Academic Press: New York, 2002.
(22) Sigel, R.; Pispas, S.; Vlassopoulos, D.; Hadjichristidis, N.; Fytas, G. *Phys. Rev. Lett.* **1999**, *83*, 4666.
(23) Forster, S.; Wenz, E.; Lindner, P. *Phys. Rev. Lett.* **1996**, *77*, 95.
(24) Laurati, M.; Stelenbrink, J.; Lund, R.; Willner, L.; Zacarelli, E.; Richter, D. *Phys. E* **2007**, *76*, 041503.
(25) Beenakker, C. W. J.; Mazur, P. *Physica A* **1984**, *126*, 349.
(26) Vlassopoulos, D.; Fytas, G. *Adv. Polym. Sci.* **2009**, 000.
(27) Likos, C. N. *Soft Matter* **2006**, *2*, 478.
(28) Vanmegen, W.; Underwood, S. M. *J. Chem. Phys.* **1989**, *91*, 552.
(29) Pusey, P. N.; Vanmegen, W. *J. Phys. (Paris)* **1983**, *44*, 285.
(30) Ottewill, R. H.; Williams, N. S. J. *Nature (London)* **1987**, *325*, 232.
(31) Michailidou, V. N., P. G.; Swan, J. H.; Brady, J. F. *Phys. Rev. Lett.* **2009**.
(32) Glendinning, A. B.; Russel, W. B. *J. Colloid Interface Sci.* **1982**, *89*, 124.
(33) Batchelor, G. K. *J. Fluid Mech.* **1976**, *74*, 1.
(34) Kopswerkhoven, M. M.; Fijnaut, H. M. *J. Chem. Phys.* **1981**, *74*, 1618.
(35) Kopswerkhoven, M. M.; Fijnaut, H. M. *J. Chem. Phys.* **1982**, *77*, 2242.

MA802878R